Journal of Magnetism and Magnetic Materials 564 (2022) 169990

Contents lists available at ScienceDirect

Journal of Magnetism and Magnetic Materials

journal homepage: www.elsevier.com/locate/jmmm

Research article

Increased Curie temperature and magnetoresistive response by modifying Fe/Mo ratio in Sr_2FeMoO_6 thin films

Naman A. Naushahi [a,b,*], I. Angervo [a], M. Saloaro [a], A. Schulman [a], H. Huhtinen [a], P. Paturi [a]

[a] Wihuri Physical Laboratory, Department of Physics and Astronomy, FI-20014 University of Turku, Finland
[b] University of Turku Graduate School (UTUGS), University of Turku, Finland

ARTICLE INFO

Keywords:
Spintronics
Spin valve
SFMO
Stoichiometry
Magnetic properties
Transport properties

ABSTRACT

We investigated the effect of deposition distance on a set of otherwise identically grown Sr_2FeMoO_6 (SFMO) thin films grown by pulsed laser deposition. Based on the detailed magnetic and transport measurements, we found that the optimal properties can be realized at longer deposition distances than earlier expected. The achieved onset Curie temperature of the order of 400 K with the middle transition value of 372 K, which are clearly the highest presented in the literature for the SFMO thin films. In addition, the increased metallicity and magnetoresistive response is observed in films deposited at longer distances. The improvements are widely discussed in the light of discovered stoichiometric imbalance between the cations Fe and Mo, which modify the magnetic interactions and thus magnetic and electric properties. Therefore, this study shows a new approach in the deposition process to provide the SFMO thin films and multilayers of high quality for future spin valve devices working at room temperature.

1. Introduction

The double perovskite Sr_2FeMoO_6 (SFMO) has attracted extensive consideration attributable to a portion of its exceptional features such as high Curie temperature T_C and high degree of spin polarization [1]. The T_C of the polycrystalline bulk SFMO is around 410 – 450 K, astonishingly high for a half metal, which enables the material being suitable for room temperature spintronics [1–3]. However, for innovative spintronic applications, a full understanding of the stoichiometry and lattice ordering of SFMO epitaxial thin films is required, especially since the thin film preparation has proven to be extremely challenging and the electric and magnetic properties of the films have been greatly deteriorated. For example, the T_C's of the SFMO films have mostly remained in the level of 350 K [4–6].

To understand the mechanisms behind the improved T_C and the magnetoresistive (MR) response together with charge carriers of 100% spin polarization, the formation of nanoscale defects in SFMO needs to be managed. As comprehensively discussed earlier, experimentally and theoretically, the roles of strain induced by the substrate, oxygen vacancies in the SFMO lattice as well as the formation of anti-site disorder (ASD) have been observed to have a great impact on the properties of the final film structures [4,7]. For example, T_C has been observed to decrease with the increased number of ASD and oxygen vacancies [7] and the substrate-induced strain has clearly a decreasing impact on T_C and saturation magnetization M_s [4,8–10]. It is well established that in SFMO ceramics the major contribution to MR arises from spin-dependent electron tunnelling across insulating grain boundaries [11]. MR is supported in thin films subjected to large biaxial compressive strain at the substrate-film interface. The origin of this phenomenon is proposed to be the presence of antiphase domain boundaries since the super-structure direction is adjusted here to the growth direction [12]. In summary, all the earlier studies have suggested that a notable changes in transport properties of SFMO films are caused by the disordering in the lattice. Thus, the ASD and especially stoichiometry between the cations Fe and Mo have an immense effect on the spin polarization, and the mobility and the density of the carriers in SFMO [13].

Pulsed laser deposition is in a key role when trying to affect on the formation of the above-mentioned defects during the film growth process [14–16]. Especially, the ejected plasma plume and its propagation through the background gas are critically dependent on the laser power density, ambient pressure of the background gas, the distance between the target and the substrate and the substrate temperature during the growth process [17]. However, laser fluence is more related to the explosive removal of the material from the target and the optimal growth temperature to synthesize the SFMO is already known [18], but the combination of background pressure and target-substrate distance remains unsettled. The optimization of SFMO thin

* Corresponding author at: Wihuri Physical Laboratory, Department of Physics and Astronomy, FI-20014 University of Turku, Finland.
E-mail address: naman.a.naushahi@utu.fi (N.A. Naushahi).

https://doi.org/10.1016/j.jmmm.2022.169990
Received 15 June 2022; Received in revised form 7 September 2022; Accepted 19 September 2022
Available online 5 October 2022

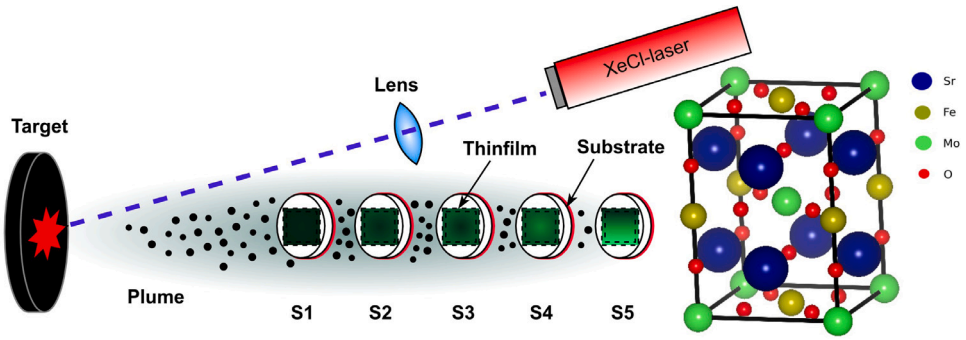

Fig. 1. Schematic illustration of the visible laser plume propagating from the target surface, including the decreasing material density with increasing deposition distance. The samples S1, S2, S3, S4 and S5 refer to the different deposition distances of 2.2, 2.7, 3.2, 3.7 and 4.2 cm where the SFMO unit cells start to epitaxially grow.

films depends on several parameters and target to substrate distance is one of the important parameter. For example, the deposition distance has been demonstrated to influence the stoichiometric balance of the material. This provides a clear variable for further deposition optimization and understanding about the effects of off-stoichiometry in SFMO thin films [19]. In our system, we have used the deposition distance (3.2 cm) for the fabrication of smoother thin films and achieved high crystallinity [18,20]. Therefore, the main objective of this work is to find the optimal deposition distance for obtaining as high as possible T_C and magnetoresistive response in the SFMO thin films, by fixing the optimized deposition temperature and atmosphere. We have addressed the effect of deposition distance and structural characteristics of the films on magnetic and magneto-transport properties. Based on the experimental results, the orientations for achieving optimal SFMO films for future applications are proposed.

2. Experimental details

Pulsed laser deposition (PLD) was used to prepare five SFMO thin films on $SrTiO_3$ (100) single crystal substrates, varying the deposition distances from the target as 2.2 cm (S1), 2.7 cm (S2), 3.2 cm (S3), 3.7 cm (S4) and 4.2 cm (S5), as schematically illustrated in Fig. 1. The deposition was carried out at 900 °C in Ar atmosphere of 9 Pa, which has earlier been shown to produce smooth and crystallographically good SFMO thin films [6]. SFMO target used in the deposition process was fabricated by a solid-state reaction method and the whole target preparation, from powder to pellet, is described in detail [18]. All the films were prepared with 2000 laser pulses and the deposition temperature was kept the same for all the films. A XeCl excimer laser with a wavelength of $\lambda = 308$ nm, a repetition rate of 5 Hz and a fluence of 1.4 J/cm^2 were utilized in the deposition procedure. For the post-annealing treatment, the films were held at a constant temperature for 10 min before being cooled down at a rate of 25 °C/min to room temperature.

Surface analysis of the deposited SFMO thin films is done with an Innova atomic force microscopy (AFM) provided by Bruker. The contact mode AFM scans of various sizes were performed at room temperature. The surface roughness of the films was determined as a root mean square (RMS) value. To determine the thicknesses of the films, the films were photolithographically patterned as stripes, over which the AFM scans were carried out. Compositional analysis of the films was effectuated with the energy dispersive spectroscopy (EDS) by using the Thermo Scientific high-resolution field emission scanning electron microscopy (FE-SEM). The data is taken at four positions on each film and the calculated average is shown in Table 2. X-ray diffraction (XRD) using Empyrean diffractometer with 5-axis goniometer Cu K_α radiation was employed to examine the structural characteristics of the films. The crystalline nature, orientation, and lattice parameters were determined by applying $\theta - 2\theta$-scans between 20° − 114°. To confirm texturing and c-axis oriented SFMO phase, $\phi - \psi$-measurements were taken for

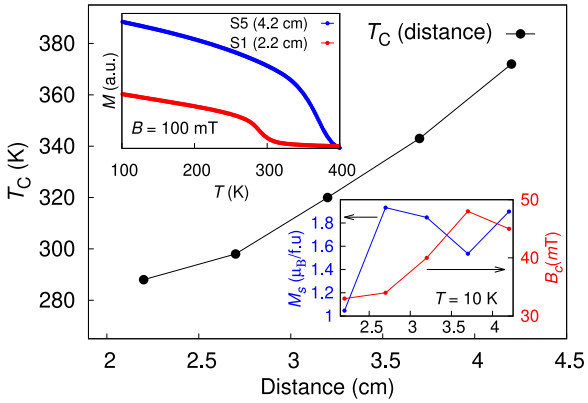

Fig. 2. The Curie temperature, T_C, as a function of deposition distance (main panel). The bottom right inset shows the saturation magnetization M_s (left-side) and the coercive field B_c (right-side) as a function of distance, determined from the hysteresis loops taken at 10 K. Top left inset shows the temperature-dependent FC magnetization curves for samples S1 and S5 measured in 100 mT field.

SFMO (204)-peak. The in-plane and out-of-plane strains of the films were calculated using the lattice parameters.

A MPMS XL SQUID magnetometer provided by Quantum Design was employed to study the magnetic properties of the films. The zero field cooled (ZFC) and field cooled (FC) magnetizations were measured between 10 K and 400 K in the field of 100 mT to determine T_C of the SFMO films. Magnetic hysteresis loops were measured between ±1 T at 10 K and 400 K. The saturation magnetization was defined as the magnetization value in 400 mT field at 10 K. In all these measurements, the external magnetic field was parallel to the plane of the film, i.e. in the (110) direction. A Quantum Design Physical Property Measurement System (PPMS) was utilized to measure the resistive properties of the films. The temperature dependence of the resistivity was measured in 0 T, 100 mT and 1 T and fields as a function of temperature from 10 K to 300 K. In these measurements, the plane of the films was parallel to the external field.

3. Results and discussion

3.1. Improvements in magnetic and resistive properties

The field cooled (FC) magnetization is presented as a function of temperature in the top left inset of Fig. 2 for samples S1 and S5. It is clear from the curves that the ferromagnetic to paramagnetic (FM-PM) transition of S5 takes place at significantly higher temperature when compared with S1. T_C is presented as a function of deposition distance in the main panel of Fig. 2. It can be clearly seen that T_C determined

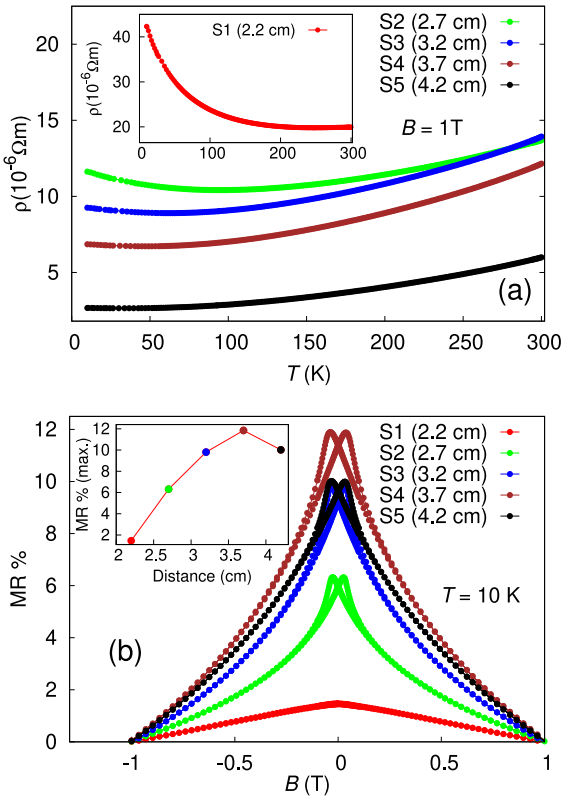

Fig. 3. (a) Temperature dependence of the resistivity change for the SFMO thin films measured in 1 T magnetic field. The inset shows the resistivity behaviour of the film fabricated at the shortest distance. (b) The magnetoresistive response of all the prepared SFMO thin films measured at 10 K. The inset shows the maximum magnetoresistive values plotted with the deposition distance.

from the first-order derivative of the FC curve has an increasing tendency with increasing deposition distance, having the highest value of 372 K at the longest deposition distance of S5, being clearly higher than the earlier reported maximum of 363 K [20]. The higher T_C values are usually explained by the result of the smaller number of ASD [21,22], but also an opposite tendency has been reported [23]. In addition, the theoretical and experimental works reported that higher oxygen vacancy concentration could increase T_C [4,24]. As will be discussed later, the change in FM-PM transition temperature can be related to modified Fe/Mo stoichiometric imbalance that affects the exchange coupling between them [25,26].

The saturation magnetization values M_s together with coercivities B_c were obtained from the hysteresis loops measured at 10 K and their deposition distance dependencies are shown in the bottom right inset of Fig. 2. Similarly to T_C, M_s values show an increasing trend at the two shortest distances S1 and S2, and approximately constant value above this. However, the M_s values are significantly lower than the theoretically calculated maximum values of 4 μ_B/f.u. This is usually explained by the disorder between the cations, where the ASD between Fe and Mo influences the magnetic and transport properties as the overlapping of orbitals would be changed by the level of ASD [27].

In Fig. 3(a), the absolute resistivities ρ of the SFMO thin films are presented as functions of temperature measured in 1 T field. The temperature dependencies of ρ at different distances differ from each other, but in spite of a small upturn at low temperatures, we obtained a minimum in ρ(T) between 50 and 100 K and a trend of metallic behaviour at the temperature range over 60 K for all the samples except S1. In S1, a full semiconductive behaviour over the entire range of temperature can be seen, being in agreement with the results reported earlier [8,9]. This behaviour is in clear contrast to the other samples, being consistent with the variable range hopping (VRH) model [28–30]. Looking at the resistivity levels of the curves, the ρ_{min} seems to decrease with increasing deposition distance and thus the most metallic behaviour can be seen in S5, where also the highest T_C is observed.

In our previous work, we have utilized a semi-empirical model, which utilizes parallel connected conduction channels, to explain the temperature dependence of resistivity [8]. The semi-conductive-like behaviour was argued to be linked to the demise of spin-polarization due to changes in the semi-conductive spin-up channel. In short, the semi-conductive-like behaviour suggests that the SFMO system might not exhibit high spin-polarization. Studies discussing VRH model, or simply the increase in resistance with decreasing temperature, often rely on the existence of secondary phases including $SrMoO_4$ and/or ASD [31–35]. Conducted studies suggest that structural defects such as ASD can change the electronic structure in SFMO and reduce the band gap [36–38]. On the other hand, $SrMoO_4$ is a parasitic phase in SFMO. Although an accurate overall understanding of resistivity upturn seems to remain somewhat elusive, the phenomenon seems to be an indication of a non-ideal SFMO system.

Magnetoresistance, MR = $(R_B - R_0)/R_0$, as a function of an applied magnetic field measured at 10 K for all the deposited thin films are shown in the main panel of Fig. 3(b), where R_B is the resistance under the applied field and R_0 is the zero-field resistance. The magnetic field dependent MR curves increase gradually with decreasing magnetic field, exhibiting clear hysteresis in the low field range and having the maxima in the MR curves around 50 mT, as also observed earlier for SFMO thin films [8,9,15,39,40]. S1 stands out from the other samples in the sense that hysteretic magnetoresistance is practically absent and the overall MR response is considerably smaller. The inset in Fig. 3(b) shows the maximum MR values obtained from all the samples of S1, S2, S3, S4 and S5. The maximum MR seems to increase almost linearly from the sample S1 of 2% with increasing deposition distance up to S4, where the maximum value of 12% is reached. Above this distance, the MR in sample S5 is already slightly diminished being ≈10%.

The low field MR is attributed to the spin-dependent scattering combined with magnetic hysteresis [1]. In addition, there may be a direct relation between this and the presence of AFM domains as a consequence of ASD [11]. The fact that S1 showed virtually no low field MR response could be related to the fact that SFMO does not exhibit significant spin-polarized carrier transport. This is in line with the argument obtained from the semi-empirical model. A slight deviation in B-site stoichiometry has a huge impact on the spin-polarization, carrier density and their mobility in SFMO. It has been reported that 30% disorder changes the MR by approximately three times. Theoretical calculations also suggested that relaxation time, group velocity and transport coefficient can be controlled by the B-site stoichiometry [41].

3.2. Distance dependent structural properties

The θ - 2θ scans were performed for all the SFMO thin films. The results showed clear (00ℓ) peaks arising from the SFMO thin films and substrates and no impurity phases were observed. The XRD results for all the samples confirm that PLD fabrication has produced phase pure thin films. As can be seen from the thickness values of the films presented in Table 1, the thickness dramatically decreases when the deposition distance is increased. The RMS roughnesses measured by AFM as averages of all the scans with different scan areas are also shown in Table 1. The smoothest films with the roughness value of ≈ 1.5 nm are deposited at the distance of 3.2 cm in S3, which actually is the earlier optimized deposition distance in this system [42]. Both the shorter and longer distances produce rougher surfaces and the increasing roughness is mainly related to the formation of the laser droplets. Since the kinetic energy of the particles depends on the distance in the laser plume, the optimal distance in terms of roughness can obviously be different than in the case of magnetic or resistive properties [43,44].

Table 1
Structural properties measured by XRD and AFM for SFMO films deposited at different distances. The thickness values t given in the last column are measured from the patterned stripes of the films and calibrated with X-ray reflection measurements (XRR).

Sample	d (cm)	a (Å)	c (Å)	ε_a (%)	ε_c (%)	$\Delta\phi$ (°)	RMS (nm)	t (nm)
S1	2.2	5.582	7.903	0.13	0.13	0.5	2.68	200
S2	2.7	5.599	7.914	0.44	0.26	0.59	1.90	150
S3	3.2	5.582	7.909	0.13	0.20	0.78	1.57	130
S4	3.7	5.562	7.905	−0.23	0.15	1.06	2.29	40
S5	4.2	5.570	7.896	−0.08	0.04	0.62	3.18	30

Table 2
The relative weight percentages of the metals Sr, Fe and Mo obtained in SFMO thin films S1_MgO, S3_MgO and S5_MgO deposited at different distances. The films for EDS analysis were deposited on MgO substrate to distinguish the role of Sr, which is also available in STO substrate.

Sample	d (cm)	Sr (%)	Mo (%)	Fe (%)
S1_MgO	2.2	48.6	27.2	24.2
S3_MgO	3.2	51.4	26.1	22.5
S5_MgO	4.2	46.8	21.6	31.6

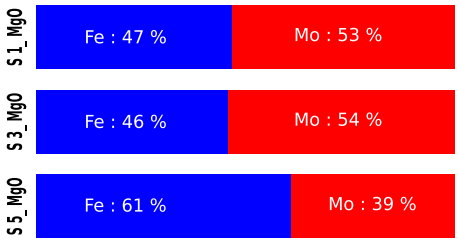

Fig. 4. Variation of the Fe/Mo ratio in films S1_MgO, S3_MgO and S5_MgO measured by EDS.

Lattice parameters a and c were obtained by fitting a symmetric Gaussian function to (336) and (008) peaks in the θ - 2θ scans, respectively [45], and the results are presented in Table 1. According to these findings, variation in the in-plane lattice parameters is insignificant although the slightly decreased values can be seen in films prepared at longer deposition distances of S4 and S5. The out-of-plane lattice parameter c is within the error bars constant at all the distances although it is slightly diminished at the longest distance of S5. However, we can conclude that all the lattice parameters in both directions are similar to the values of polycrystalline samples and thin films reported in the literature [9,46–49].

The in-plane and out-of-plane strain values ε_a and ε_c were calculated as $\varepsilon_{a,c} = (l_{a,c} - l_{SFMO})/l_{SFMO}$, where $l_{a,c}$ is the measured SFMO lattice parameters a and c, and l_{SFMO} represents the unstrained SFMO lattice parameter according to [50]. As can be seen in Table 1, the in-plane strain values ε_a are positive at shorter deposition distances, while above the distance 3.2 cm of S3, the values of ε_a are negative. Since the in-plane lattice mismatch between the STO substrate and the nominal SFMO is only about 1% inducing a compressive strain at the substrate-film interface, we can assume that the strain relaxation is still underway in thin films at longer deposition distances, having slightly compressed in-plane unit cell, while the remarkably thicker films of S1, S2 and S3 have enlarged unit cell when compared with the nominal one. The in-plane broadening of the XRD peaks was determined as $\Delta\phi$, measuring a full width at half maximum (FWHM) of the peaks by fitting the symmetric Gaussian function with the $2\theta - \phi$ scan corresponds to the 2θ value of the highest intensity of the SFMO (204) peak. The value of $\Delta\phi$ obtained by Gaussian fit was almost linearly increasing up to the distance 3.7 cm of S4, above which it starts to decrease again. The broadening of $\Delta\phi$ is usually connected to the formation of low-angle grain boundaries and other in-plane defects in the SFMO lattice, which again could induce the domain wall pinning in the films [4,20].

3.3. Effect of imbalance between cations Fe and Mo

To verify the stoichiometric effect between the elements in SFMO, we have measured the atomic weight percentages of three films, deposited on MgO substrate, by EDS. Variation of stoichiometry at four different positions on the films was found to be within the detection limit. Therefore, we can assume that the films are homogeneous. In Table 2, we show the average weight percentages of Sr, Mo and Fe in the films deposited at different distances of S1_MgO, S3_MgO and S5_MgO. As can be seen, the amount of Sr is somewhat constant and close to the expected nominal value of 50% at all the distances, while Mo has clearly a decreasing trend with increased deposition distance. The most obvious difference can be seen in Fe, where its amount is increased by over 35% at the longest deposition distance of S5_MgO. To solidify this change, we present a bar graph ratio between the cations Mo and Fe as a function of deposition distance, as observed with the quantitative EDS analysis. In Fig. 4, it is clearly observed that the off-stoichiometry between Fe and Mo is significant in samples deposited at different distances, especially at the longest distance of S5_MgO, where the nominal ratio of Fe/Mo = 50%/50% is changed to the value of 60%/40%. Since no secondary phases have been observed in our quality monitoring, the results suggest possible but considerable, off-stoichiometry SFMO phase of S5_MgO. There is a possibility that off-stoichiometry in SFMO might lead to ASD-like disorder where Mo is replaced with Fe. The ASD in SFMO has a deteriorating effect on SFMO attributes [10,51,52], but we do not observe the deterioration of sample quality with enhanced off-stoichiometry. This could mean that despite the off-stoichiometry in our samples, this has not produced significant ASD, which would diminish the sample quality.

In SFMO thin films, the deposition conditions such as the growth temperature and deposition atmosphere have been observed to have a great impact on the disorder formation in the Fe-Mo sublattice [40,53,54], and ASD has shown to decrease T_C and saturation magnetization, weakening also the spin-polarization [21,37,55–57]. This is linked to a strong superexchange interaction that may couple the spins of iron ions occupying adjacent B sites. However, the wide range of magnetic and electric results revealed that an ideal design for SFMO films is feasible by optimizing the deposition conditions [25,26,58].

The stoichiometric imbalance between Fe and Mo in SFMO is assisted by the defects of ASD, which leads to the formation of Fe–O–Fe_{Mo} and Mo–O–Mo_{Fe} bonds [59]. The schematic illustration of the ASD and Fe/Mo imbalance is shown in Fig. 5(a). The imbalance can be observed as the Fe substituted on a Mo site having spin ↑, which again induces the superexchange interaction [60]. A schematic description of the superexchange interactions is presented in Fig. 5(b). The antiferromagnetic coupling between Fe^{3+} and Mo^{5+} ions are responsible for the ferrimagnetic ordering in SFMO [61]. In addition, it has been shown that Fe can also have a valence of 2+instead of 3+and that Mo can have a valence of 6+instead of 5+ [62]. Mo^{6+} has a zero net magnetic moment. The valence mixing, Fe^{3+}–O–Mo–O–Fe^{2+} can also experience double exchange, involving itinerant electrons. The valence mixing of SFMO in Fe and Mo has been confirmed experimentally [63–67].

While it is indeed reported that Fe or Mo enriched SFMO induces ASD formation [68], it is also demonstrated that the stoichiometric imbalance with Fe rich composition may preserve the spin polarization [57,68,69], while the excess of Mo eventually becomes disadvantageous [41,57,68–70]. Since we have observed excess Fe in S5_MgO,

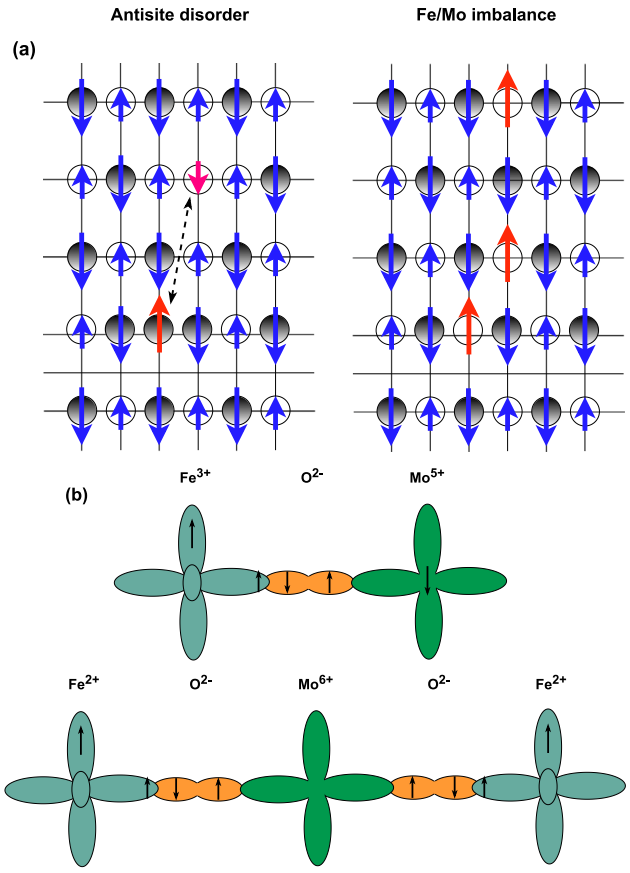

Fig. 5. (a) Schematic picture of Mo/Fe ASD (left), where one Mo atom is replaced with Fe atom and vice versa and their stoichiometry imbalance (right), where the excess of Fe atoms are placed on the Mo sites. The solid circles represent Fe and open circles represent Mo, while the arrows represent the magnetic moments of the atoms. (b) Schematic figure of the superexchange interactions in the possible Fe^{3+} Mo^{5+} and Fe^{2+} Mo^{6+} configurations of SFMO.

which simultaneously preserves low field MR response and shows more metallic temperature dependence, the results seem to be well within the arguments presented in the literature. Although we have demonstrated a slightly Mo rich phase in S1_MgO and S3_MgO, the stoichiometric imbalance is not as significant as with Fe rich S5_MgO. For this reason, it cannot be established, at least convincingly, that additional Mo causes the deterioration of desirable attributes in S1. However, we cannot fully exclude this possibility. It should be noted that additional reports also argue that any deviation from the stoichiometric balance or excess Fe in SFMO can become deteriorating [71].

The underlying mechanisms behind the increased T_C and retained low field MR, hence retained spin-polarization, are of course direct consequences of crystalline structure and elemental exchange interactions due to immediate orbital vicinity. A detailed explanation for the phenomena is sometimes obtained with different theoretical approaches and the remarks are not always consistent. It is reported that simple ASD [4] and ASD due to excess Fe can have a stabilizing effect on magnetization against temperature [57]. This is due to strong antiferromagnetic superexchange interaction in ASD defects binding the defect-free spins [57]. However, when realizing double-exchange-like interaction in defect-free SFMO, in order to obtain higher T_C, SFMO might require carrier doping [57,72], since substitution of Mo with Fe is a trade resulting in fewer itinerant electrons. In a different exchange interaction case, it is pointed out that the RKKY theory makes the same claim, as an increase in the concentration of free carriers results in an increase in density of states at the Fermi level, as well as an increase in the exchange interaction and thus T_C [27,66,73–76].

Although, we have focused our attention on stoichiometric imbalance and its influences on SFMO, we should keep in mind that various point defects and lattice distortion are likely playing their role. For example, we have evidences of higher compressive in-plane strain in S5 and S4, the two thinnest films in the set. The stabilizing effect of strain for additional ASD might prevent the dramatic loss of spin polarization [77]. However, the overall trend in strain alone cannot be used to explain the results of enhanced magnetic properties with increased deposition distance. This could be related to the fact that low field MR showed a slight decrease in S5, while the maximal MR was realized with S4 combined with a slightly smaller T_C compared to S5. In addition, oxygen vacancies have been demonstrated to increase T_C and maintaining spin polarization [24]. To conclude, we crystallize the fact that Fe/Mo concentration varies significantly. We used the PLD method and deposited films at different distances. We can expect this to modify the elemental ratio as there is a mass difference between Fe and Mo atoms. In the deposition process, the flow of atoms towards the substrate can result in a highly off-stoichiometric material [19]. Since the deposition is otherwise identical, we do not expect significant variation in other factors such as the ASD and oxygen vacancy [7]. For this reason, these defects do not seem to account for the trend of a substantial increase in T_C and enhanced magnetoresistive response. However, the observed stoichiometric changes can be used to argue for the demonstrated phenomenon.

4. Conclusions

We have fabricated a series of SFMO thin films on single crystal STO substrates, by varying the deposition distance, and the samples were systematically characterized by the structural, magnetic and resistivity methods. Based on our experimental observations, the films exhibit high T_C, well above room temperature and the T_C is observed to increase with increasing deposition distance. In addition, the metallicity as well as low-field magnetoresistance have been observed in films deposited at higher distances than earlier expected. Based on EDX measurements, we have clear results that longer deposition distance has induced off-stoichiometry between Fe and Mo. In addition, relevant structural imperfections were discussed accordingly. We suggest that the improved properties could be connected to the magnetic instabilities caused by the structural imperfections in the lattice due to the stoichiometric imbalance of the Fe/Mo cations. Therefore, we can conclude that the choice of distance or otherwise artificially modified cationic ratio in SFMO are in a crucial role when trying to optimize the SFMO thin films for various applications in future spintronic and magnetoresistive environments.

CRediT authorship contribution statement

Naman A. Naushahi: Methodology, Data curation, Investigation, Software, Validation, Writing – original draft, Visualization. **I. Angervo:** Software, Investigation, Validation, Writing – review & editing. **M. Saloaro:** Supervision, Investigation, Resources. **A. Schulman:** Investigation, Resources. **H. Huhtinen:** Supervision, Reviewing and editing, Validation. **P. Paturi:** Supervision, Project administration, Formal analysis, Reviewing and editing.

Declaration of competing interest

The authors declare that they have no known competing financial interests or personal relationships that could have appeared to influence the work reported in this paper.

Data availability

No data was used for the research described in the article.

Acknowledgements

The Jenny and Antti Wihuri Foundation are acknowledged for financial support. The EDUFI funding by the Finnish National Agency for Education, Finland made the project possible.

References

[1] K.I. Kobayashi, T. Kimura, H. Sawada, K. Terakura, Y. Tokura, Nature 395 (1998) 677.
[2] M. Bibes, K. Bouzehouane, A. Barthelemy, M. Besse, S. Fusil, M. Bowen, P. Seneor, J. Carrey, V. Cros, A. Vaures, J.-P. Contour, A. Fert, Appl. Phys. Lett. 83 (2003) 2629.
[3] Y. Tomioka, T. Okuda, Y. Okimoto, R. Kumai, K.-I. Kobayashi, Y. Tokura, Phys. Rev. B 61 (2000) 422.
[4] M. Saloaro, M. Hoffmann, W.A. Adeagbo, S. Granroth, H. Deniz, H. Palonen, H. Huhtinen, S. Majumdar, P. Laukkanen, W. Hergert, A. Ernst, P. Paturi, ACS Appl. Mater. Interfaces 8 (2016) 20440.
[5] D. Sanchez, N. Auth, G. Jakob, J.L. Martinez, M. Garcia-Hernandes, J. Magn. Magn. Mater. 294 (2005) e119.
[6] P. Paturi, M. Metsänoja, H. Huhtinen, Thin Solid Films 519 (2011) 8047.
[7] M. Saloaro, M.O. Liedke, I. Angervo, M. Butterling, E. Hirschmann, A. Wagner, H. Huhtinen, P. Paturi, J. Magn. Magn. Mater. 540 (2021) 168454, 1–6.
[8] M. Saloaro, S. Majumdar, H. Huhtinen, P. Paturi, J. Phys.: Condens. Matter 24 (2012) 366003.
[9] M. Saloaro, S. Majumdar, H. Huhtinen, P. Paturi, EPJ Web Conf. 40 (2013) 15012.
[10] M. Saloaro, H. Deniz, H. Huhtinen, H. Palonen, S. Majumdar, P. Paturi, J. Phys.: Condens. Matter 27 (2015) 386001, 1–11.
[11] D.D. Sarma, S. Ray, K. Tanaka, M. Kobayashi, A. Fujimori, P. Sanyal, H.R. Krishnamurthy, C. Dasgupta, Phys. Rev. Lett. 98 (2007) 157205.
[12] G. Suchaneck, N. Kalanda, E. Artsiukh, G. Gerlach, Phys. Status Solidi b 257 (2020) 1900312.
[13] J.F. Wang, T.F. Shi, Z.T. Zhuang, Q.Q. Gao, Y.M. Zhang, RSC Adv. 8 (51) (2018) 29071–29077.
[14] H. Asano, S.B. Ogale, J. Garrison, A. Orozco, Y.H. Li, E. Li, V. Smolyaninova, C. Galley, M. Downes, M. Rajeswari, R. Ramesh, T. Venkatesan, Appl. Phys. Lett. 74 (1999) 3696.
[15] T. Manako, M. Izumi, Y. Konishi, K.-I. Kobayashi, M. Kawasaki, Y. Tokura, Appl. Phys. Lett. 74 (1999) 2215.
[16] H.Q. Yin, J.-S. Zhou, J.-P. Zhou, R. Dass, J.T. McDevitt, J.B. Goodenough, J. Appl. Phys. 75 (1999) 2812.
[17] D.B. Chrisey, G.K. Hubler, John Wiley Sons Inc, 1994.
[18] I. Angervo, M. Saloaro, H. Huhtinen, P. Paturi, Appl. Surf. Sci. 422 (2017) 682.
[19] J. Schou, Appl. Surf. Sci. 255 (2009) 5191.
[20] I. Angervo, M. Saloaro, J. Tikkanen, H. Huhtinen, P. Paturi, Appl. Surf. Sci. 396 (2017) 754.
[21] A.S. Ogale, S.B. Ogale, R. Ramesh, T. Venkatesan, Appl. Phys. Lett. 75 (1999) 537.
[22] B.J. Park, H. Han, J. Kim, Y.J. Kim, C.S. Kim, B.W. Lee, J. Magn. Magn. Mater. 272-276 (2004) 1851.
[23] J.L. Alonso, L.A. Fernández, F. Guinea, F. Lesmes, V. Martín-Mayor, Phys. Rev. B 67 (2003) 214423.
[24] M. Hoffmann, V.N. Antonov, L.V. Bekenov, K. Kokko, W. Hergert, A. Ernst, J. Phys. Condens. Matter 30 (2018) 305801.
[25] T.L. Meyer, M. Dixit, R.E.A. Williams, M.A. Susner, H.L. Fraser, D.W. McComb, M.D. Sumption, T.R. Lemberger, P.M. Woodward, J. Appl. Phys. 116 (2014) 013905.
[26] L. Balcells, J. Navarro, M. Bibes, A. Roig, B. Martinez, J. Foncuberta, Appl. Phys. Lett. 78 (2001) 781.
[27] N. Kalanda, V. Turchenko, D. Karpinsky, S. Demyanov, M. Yarmolich, M. Balasoiu, N. Lupu, S. Tyutyunnikov, N.A. Sobolev, Phys. Status Solidi b 256 (2019) 1800278.
[28] N.F. Mott, Phil. Mag. 19 (1969) 835.
[29] G. Popov, M. Greenblatt, M. Croft, Phys. Rev. B 67 (2003) 024406.
[30] A. Poddar, S. Das, B. Chattopadhyay, J. Appl. Phys. 95 (2004) 6261–6267.
[31] W. Westerburg, F. Martin, S. Friedrich, G. Jakob, J. Appl. Phys. 86 (1999) 2173.
[32] W. Westerburg, D. Reisinger, G. Jakob, Phys. Rev. B 62 (2000) R767.
[33] G. Suchaneck, N. Kalanda, E. Artiukh, M. Yarmolich, N.A. Sobolev, J. Alloy. Compd. 860 (2021) 158526.
[34] M.V. Yarmolich, N.A. Kalanda, I.A. Svito, A.L. Zhaludkevich, N.A. Sobolev, Mod. Electron. Mater. 2 (2016) 106.
[35] Y. Zhai, J. Qiao, G. Huo, S. Han, J. Magn. Magn. Mater. 324 (2012) 2006.
[36] B. Aguilar, O. Navarro, M. Avignon, Europhys. Lett. 88 (2009) 67003.
[37] T. Saha-Dasgupta, D.D. Sarma, Phys. Rev. B 64 (2001) 064408.
[38] R.P. Panguluri, S. Xu, Y. Moritomo, I.V. Solovyev, B. Nadgorny, Appl. Phys. Lett. 94 (2009) 012501.
[39] M. Metsänoja, S. Majumdar, H. Huhtinen, P. Paturi, J. Supercond. Nov. Magn. 25 (2012) 829.
[40] D. Sánchez, M. García-Hernández, N. Auth, G. Jakob, J. Appl. Phys. 96 (2004) 2736.
[41] N. Kumar, R. Gupta, R. Kaur, D. Oka, S. Kakkar, S. Kumar, S. Singh, T. Fukumura, C. Bera, S. Chakraverty, ACS Appl. Electron. Mater. 3 (2021) 597–604.
[42] H. Palonen, H. Huhtinen, M.A. Shakhov, P. Paturi, Supercond. Sci. Technol. 26 (2013) 045003, 1–5.
[43] R.K. Singh, J. Narayan, Phys. Rev. B 41 (1990) 8843.
[44] J.M.O. Esteban, Prensas de la Universidad de Zaragoza, 2010.
[45] J.B. Nelson, D.P. Riley, Proc. Phys. Soc. 57 (1945) 160–177.
[46] T. Fix, D. Stoeffler, S. Colis, C. Ullhaq, G. Versini, J.P. Vola, F. Huber, A. Dinia, J. Appl. Phys. 98 (2005) 023712.
[47] R. Boucher, J. Phys. Chem. Solids 66 (2005) 1020.
[48] H. Jalili, N.F. Heinig, K.T. Leung, J. Chem. Phys. 132 (2010) 204701.
[49] D. Kumar, D. Kaur, Phys. B 405 (2010) 3259.
[50] S. Nakamura, K. Oikawa, J. Phys. Soc. Japan 72 (2003) 3123.
[51] D. Stoeffler, S. Colis, Mater. Sci. Eng. B 126 (2006) 133.
[52] D. Stoeffler, S. Colis, J. Phys.: Condens. Matter 17 (2005) 6415.
[53] J. Santiso, A. Figueras, J. Fraxedas, Surf. Interface Anal. 33 (2002) 676.
[54] D.-Y. Kim, J.S. Kim, B.H. Park, J.-K. Lee, J.H. Kim, J.H. Lee, J. Chang, H.-J. Kim, I. Kim, Y.D. Park, Appl. Phys. Lett. 84 (2004) 5037.
[55] C. Meneghini, S. Ray, F. Liscio, F. Bardelli, S. Mobilio, D.D. Sarma, Phys. Rev. Lett. 103 (2009) 046403.
[56] T.-Y. Cai, Z.-Y. Li, J. Phys.: Condens. Matter 16 (2004) 3737.
[57] O. Erten, O.N. Meetei, A. Mukherjee, M. Randeria, N. Trivedi, P. Woodward, Phys. Rev. Lett. 107 (2011) 257201.
[58] L. Harnagea, P. Berthet, J. Solid State Chem. 222 (2015) 115.
[59] R. Mishra, O.D. Restrepo, P.M. Woodward, W. Windl, Chem. Mater. 22 (2010) 6092.
[60] A.M. Reyes, J. Chem. Phys. 120 (2016) 4048–4052.
[61] B. García-Landa, C. Ritter, M.R. Iarra, J. Blasco, P.A. Algarbel, R. Mahendiran, J. García, Solid State Commun. 110 (1999) 435.
[62] J. Navarro, J. Fontcuberta, M. Izquierdo, J. Avila, M.C. Asensio, Phys. Rev. B. 70 (2004) 054423.
[63] J.H. Kim, S.C. Wi, S. Yoon, B.J. Suh, J.-S. Kang, S.W. Han, K.H. Kim, A. Sekiyama, S. Kasai, S. Suga, C. Hwang, C.G. Olson, B.J. Park, B.W. Lee, J. Korean Phys. Soc. 43 (2003) 416.
[64] J.S. Kang, J.H. Kim, A. Sekiyama, S. Kasai, S. Suga, S.W. Han, K.H. Kim, T. Muro, Y. Saitoh, C. Hwang, C.G. Olson, B.J.P.B.W. Lee, J.H. Shim, J.H. Park, B.I. Min, Phys. Rev. B 66 (2002).
[65] M. Rutkowski, A.J. Hauser, F.Y. Yang, R. Ricciardo, T. Meyer, P.M. Woodward, A. Holcombe, P.A. Morris, L.J. Brillson, J. Vac. Sci. Technol. A. 28 (2010) 1240.
[66] J. Lindén, T. Yamamoto, M. Karppinen, H. Yamauchi, Appl. Phys. Lett. 76 (2000) 2925.
[67] T.-Y. Cai, Z.-Y. Li, J. Phys.: Condens. Matter 16 (2004) 3737.
[68] R. Mishra, O.D. Restrepo, P.M. Woodward, W. Windl, Chem. Mater. 22 (2010) 6092.
[69] J. Suárez, F. Estrada, O. Navarro, M. Avignon, Eur. Phys. J. B 84 (2011) 53.
[70] J.F. Wang, Y.M. Zhang, RSC Adv. 7 (2017) 26185.
[71] Y. Markandeya, K. Suresh, G. Bhikshamaiah, J. Alloys Compd. 509 (2011) 9598–9603.
[72] J. Navarro, C. Frontera, L. Balcells, B. Martinez, J. Fontcuberta, Phys. Rev. B 64 (2001) 092411.
[73] D.D. Sarma, P. Mahadevan, T. Saha-Dasgupta, S. Ray, A. Kumar, Phys. Rev. Lett. 85 (2000) 2549.
[74] S. Ray, A. Kumar, D.D. Sarma, R. Cimino, S. Turchini, S. Zennaro, N. Zema, Phys. Rev. Lett. 87 (2001) 097204.
[75] D. Sarma, Curr. Opin. Solid State Mater. Sci. 5 (2001) 261–268.
[76] M. Besse, V. Cros, A. Barthélémy, H. Jaffrès, J. Vogel, F. Petroff, A. Mirone, A. Tagliaferri, P. Bencok, P. Decorse, P. Berthet, Z. Szotek, W.M. Temmerman, S.S. Dhesi, N.B. Brookes, A. Rogalev, A. Fert, Europhys. Lett. 60 (2002) 608.
[77] W.A. Adeagbo, M. Hoffmann, A. Ernst, W. Hergert, M. Saloaro, P. Paturi, K. Kokko, Phys. Rev. Mater. 2 (2018) 083604.